Computational analysis of image-based drug profiling predicts synergistic drug combinations: Applications in triple-negative breast cancer

CrossMark

*Miriam B. Brandl[a,b,c], Eddy Pasquier[a,d], Fuhai Li[c], Dominik Beck[e], Sufang Zhang[c], Hong Zhao[c,**,1], Maria Kavallaris[a,f,*,1,2], Stephen T.C. Wong[c,2]*

[a]Children's Cancer Institute Australia, Lowy Cancer Research Centre, UNSW, Randwick, NSW, Australia
[b]School of Engineering and Information Technology, University of New South Wales, Canberra, ACT, 2600, Australia
[c]Department of Systems Medicine and Bioengineering, Houston Methodist Research Institute,
Weill Cornell Medical College of Cornell University, Houston, TX, 77030, USA
[d]Metronomics Global Health Initiative, Marseille, France
[e]Lowy Cancer Research Centre and the Prince of Wales Clinical School, University of New South Wales,
Sydney, Australia
[f]ARC Centre of Excellence in Convergent Bio-Nano Science and Technology, Australian Centre for NanoMedicine,
University of New South Wales, NSW, 2052, Australia

ARTICLE INFO

ABSTRACT

An imaged-based profiling and analysis system was developed to predict clinically effective synergistic drug combinations that could accelerate the identification of effective multi-drug therapies for the treatment of triple-negative breast cancer and other challenging malignancies. The identification of effective drug combinations for the treatment of triple-negative breast cancer (TNBC) was achieved by integrating high-content screening, computational analysis, and experimental biology. The approach was based on altered cellular phenotypes induced by 55 FDA-approved drugs and biologically active compounds, acquired using fluorescence microscopy and retained in multivariate compound profiles. Dissimilarities between compound profiles guided the identification of 5 combinations, which were assessed for qualitative interaction on TNBC cell growth. The combination of the microtubule-targeting drug vinblastine with KSP/Eg5 motor protein inhibitors monastrol or ispinesib showed potent synergism in 3 independent TNBC cell lines, which was not substantiated in normal fibroblasts. The synergistic interaction was mediated by an increase in mitotic arrest with cells demonstrating typical ispinesib-induced monopolar mitotic spindles, which translated into enhanced apoptosis induction. The antitumour activity of the combination vinblastine/ispinesib was confirmed in an orthotopic mouse model of TNBC. Compared to single drug treatment, combination treatment significantly

reduced tumour growth without causing increased toxicity. Image-based profiling and analysis led to the rapid discovery of a drug combination effective against TNBC *in vitro* and *in vivo*, and has the potential to lead to the development of new therapeutic options in other hard-to-treat cancers.

1. Introduction

Multi-drug regimens are the leading treatment for cancers since single agent chemotherapies often have limited antitumour activity and have been linked to drug resistance (Ramaswamy, 2007; Zimmermann et al., 2007). The development of these treatments has been increasingly laborious due to the plethora of potential combinations available (Zinner et al., 2009). Thus, the majority of existing combination therapies were developed empirically based on clinical experience (Borisy et al., 2003; Zimmermann et al., 2007). The discovery of new drug combinations from a system-oriented angle has only recently received increasing attention. Mathematical models and computational approaches, such as optimisation and search algorithms, were successfully applied to hasten the identification of effective drug combinations (Calzolari et al., 2008; Wong et al., 2008; Zinner et al., 2009). In addition, functional interaction models reliably predicted perturbation effects in signalling pathways and changes required to obtain a favourable outcome (Nelander et al., 2008). However, in-depth assessment of identified combinations and translation to clinical trials remain to be realised.

The development of new and effective combination treatments is crucial to improve the outcome of patients with aggressive malignancies such as triple-negative breast cancer (TNBC). This breast cancer subtype is associated with young patient age and reduced progression-free and overall survival (Haffty et al., 2006; Liedtke et al., 2008). The dismal clinical outcome is mainly attributed to intrinsic and acquired drug resistance, and the absence of key molecular markers of breast cancer, which provide valuable therapeutic targets for other breast cancer subtypes (Reis-Filho and Tutt, 2008). TNBC was found to be generally more responsive to chemotherapy than other subtypes (Carey et al., 2007; Liedtke et al., 2008); however, these therapies remain suboptimal as patients without complete response have significantly shorter overall survival (Carey et al., 2007). Hence, the development of novel combination chemotherapies for treatment of TNBC is essential in order to increase patient survival rates.

The presented study identifies novel drug combinations based on the integration of high-content screening (HCS), computational, and experimental biology. HCS facilitated the automatic extraction of compound-induced phenotypes from fluorescence images of TNBC cells. Determination of compound profiles allowed for the identification of compound pairs with either very similar or distinct phenotypic outcomes, which were further assessed for synergistic interactions in *in vitro* and *in vivo* models of TNBC.

2. Materials and methods

2.1. Cell culture

MDA-MB-231-luc-D3H2LN cells (Caliper, Hopkinton, MA, USA) were cultured in DMEM medium supplemented with 10% FBS, 1% L-glutamate, 1% Na-pyruvate, 1% penicillin/streptomycin, 1% non-essential amino acid and 0.1% zeocin. MDA-MB-231 cells were maintained in DMEM (Invitrogen, Mount Waverley, Australia) supplemented with 10% FCS, 1% L-glutamate, 1% Na-pyruvate, 1% penicillin/streptomycin, and 1% non-essential amino acid. MDA-MB-468 and BT-549 cells were grown in RPMI (Invitrogen) containing 10% FCS, which was additionally plied with 0.023 IU/ml insulin for BT549 cells. MRC-5 lung fibroblasts were grown in MEM (Invitrogen) supplemented with 10% FCS, 2% sodium bicarbonate, 1% NEAA, 1% sodium pyruvate, and 1% L-glutamine. Cell lines were grown as monolayers in a humidified atmosphere at 37 °C and in 5% CO_2. The ratio of cells to well surface and compound volume was kept constant in all experiments.

2.2. Compounds

Compounds for HCS (10 mM in DMSO) were purchased from Sigma (St. Louis, MO, USA) and Tocris bioscience (Ellisville, MO, USA). Stock solutions of 50 mM monastrol (Tocris Bioscience, Bristol, UK) and 10 mM ispinesib (Selleck, Scoresby, VIC, Australia) were prepared in DMSO, and stored at −20 °C. Clinical grade vinblastine sulphate (1.1 mM) (David Bull Laboratories, Melbourne, VIC, Australia) was stored at 4 °C. For further use, compounds were diluted in the respective media.

2.3. Fluorescence staining and image acquisition

MDA-MB-231-luc-D3H2LN cells ($5*10^3$ cells/well) were grown on poly-D-lysine coated black wall 96-well plates prior to compound exposure (0.1, 1.0 and 10 μM). After 24 h immunostaining with multifluorescent markers for DNA, microtubule and actin following standard methods using the Cellomics HCS Cytoskeleton Rearrangement Kit (Thermo, Rockford, USA) was conducted. Briefly, cells were first fixed and permeabilized using formaldehyde (3.7%), before incubation with primary antibody solution containing DY554-phalloidin and tubulin primary antibody, followed by incubation with the secondary antibody solution containing DyLight 649 Goat Anti-Mouse and DAPI. Fluorescence images were captured using an Olympus IX81 microscope and a 40X objective. Images of channels for DAPI (DNA), DY554 (F-actin), and DyLight 649 (tubulin) were acquired for at least 4 different positions in wells.

2.4. Image segmentation and feature extraction

Image segmentation was conducted as previously described (Li et al., 2007). In brief, first nuclei segmentation was performed using adaptive thresholding of the DNA channel and watershed segmentation of distance-transformed images. Then over-segmentation was corrected and dead nuclei were removed. A fuzzy c-means threshold algorithm separated the F-actin channel from the background before cytoplasm was segmented on basis of nuclei and F-actin channels. Segmentation results were subsequently assessed for over-segmentation (Li et al., 2007). Segmented cells were characterised by phenotypic descriptors from 6 feature categories (Gabor wavelet, CDF 9/7 wavelet, Haralick co-occurrence, Zernike moments, region properties and shape descriptors) yielding feature vectors of 211-dimensions (Wang et al., 2009). Features were mapped into a matrix and standardized to a mean of zero and standard deviation of unity to account for different feature scales.

2.5. Multivariate image-based compound profiling

Compound-induced phenotypic changes entailed a discrepancy between treated and untreated cell populations in the multidimensional feature space. A support vector machine (SVM) was used to compute optimal hyperplanes to separate these populations (Loo et al., 2006, 2007). Hyperplanes were computed using LIBSVM version 2.89 (Chang and Lin, 2001) and based on the decision function (linear kernel, cost = 1):

$$f^k(C_i) = \langle W^k, C_i \rangle + b^k \tag{1}$$

In Equation (1), $\langle , \rangle$ denotes the dot product in the Euclidean space R^m and b^k is the bias term. Depending on the outcome of the decision function, a cell C_i was either classified to the group of treated or untreated cells (Loo et al., 2006). The prediction power of the classifier was determined by leave-one-out, 2-, 5-, and 10-fold cross-validation (CV) experiments. The orientation of the weight vector W^k described the compound-induced phenotypic change. Therefore, scaled weight vectors directed towards the population of the treated cells were employed as multivariate profiles (Loo et al., 2007). Final profiles and classification accuracies were computed from 50 resampling experiments of 2-fold CV, resulting in 152 compound profiles, 55 for concentrations of 0.1 and 1.0 μM, and 42 for 10.0 μM.

2.6. Computation of phenotypic dissimilarities

Differences between compound induced phenotypes were determined using the dissimilarities between profiles:

$$d_{p_{k_c}, p k'_c} = 1 - \frac{p_{k_c}^T * p_{k'_c}}{\sqrt{(p_{k_c}^T * p_{k_c}) * (p_{k'_c}^T * p_{k'_c})}} \tag{2}$$

In Equation (2), p_{kc} and p'_{k_c} denote profiles for compounds k_c and k'_c at either the same, or different dosage c with $c = 1,2,3$. $d_{p_{k_c}, p_{k'_c}}$ is the profile dissimilarity reflecting the differences between compound-induced cellular phenotypes (Loo et al., 2007). Profile pairs were defined as similar or dissimilar if their dissimilarity was either smaller or larger than their average

dissimilarity to all 152 profiles, respectively. Compound pairs with dissimilarities fulfilling either of these criteria for more than half of the profile pairs were considered as combination candidates with the potential to induce synergy.

2.7. Growth inhibition assays

Treatment effects on MDA-MB-231-luc growth inhibition were assessed using a bioluminescence (BLI) assay. Luciferin was added to 96-well plates, photon emission measured after 48 and 72 h using the Xenogen Imaging System (IVIS 200), and data analysed using the software Living Image 3.1 (PerkinElmer, Massachusetts, USA). Growth inhibition of other cell lines was measured on the basis of metabolic activity of cells using an Alamar blue assay and spectrophotometric analysis. Briefly, cells were plated in clear transparent 96-well plates at optimized cell densities of $3–5 \times 10^3$ cells/well for TNBC cell lines and 3×10^4 cells/well for MRC-5 cells 24 h prior to treatment. If required DMSO carrier activities exceeding concentrations of 0.1% were accounted for.

2.8. Quantification of combination effect

Two different models were used to quantify the effect of combinations. The Excess Over the Highest Single Agent (EOHSA) represents the difference in cell growth inhibition between the combination treatment and the most effective single compound at the corresponding concentration (Borisy et al., 2003; Simmons et al., 2014). It was calculated by subtracting the greater effect induced by the single compounds from that of the combination, and subsequently visualized using surface plots. While this model focuses on the effect of individual concentrations, the combination index (CI) theorem accounts for the dose response of single drugs to determine the combination effect (Chou and Talalay, 1984). The resultant equation for the CI is as follows:

$$CI = \frac{D_1}{D_{x1}} + \frac{D_2}{D_{x2}} \tag{3}$$

In Equation (3), D_1 and D_2 denote the doses of compound 1 and compound 2 required to reach an effect of x % as single treatment, while Dx_1 and Dx_2 are the doses needed in combination to inhibit x%, respectively (Chou and Talalay, 1984). Combinations were examined for induction of antagonism (CI > 1.1), additivity (0.9 < CI < 1.1), synergy (CI < 0.9) and strong synergy (CI < 0.3).

2.9. Cell cycle analysis and detection of apoptosis

MDA-MB-231 cells were cultured in T25 flasks and treated with single compounds or the combination for 24 and 48 h for cell cycle analysis and apoptosis assay, respectively. For cell cycle analysis, floating and adherent cell populations were collected and fixed in 70% methanol just before incubation with propidium iodide (PI) and RNase for 15 min in the dark. For apoptosis detection, cell pellets containing adherent and floating cells were resuspended in binding buffer containing Annexin V-FITC and PI (BD Bioscience, North Ryde, NSW, Australia) and incubated for 15 min in the dark. DNA content and apoptosis induction were immediately determined by

flow cytometry analysis (FACSCalibur, BD Biosciences, North Ryde, Australia). Cell cycle and apoptosis data were analysed using FlowJo Version 7.6.5 (TreeStar, Inc.).

2.10. Immunofluorescence staining of microtubules

MDA-MB-231 cells were seeded on 8-well Permanox Lab-Tek chamber slides (Applied Biosystems, Mulgrave, Australia) and treated 24 h later with different concentrations of ispinesib, vinblastine or the combination. After 24 h drug incubation, cells were fixed and permeabilized in 100% methanol at 20 °C for 15 min and blocked with 10% FCS for 30 min. Microtubules were then stained with anti-βI-tubulin primary antibody (Abcam, Cambridge, UK), followed by Alexa Fluor 488 anti-mouse secondary antibody (Invitrogen, Mount Waverley, Australia). All slides were mounted on coverslips with ProLong Gold anti-fade reagent containing DAPI (Invitrogen) and imaged using the 63X oil-immersion objective of an Axiovert 200 M fluorescent microscope coupled to an AxioCamMR3 camera driven by the AxioVision 4.8 software (Carl Zeiss, North Ryde, Australia). At least 350 cells were counted per condition to determine the percentage of cells in interphase and mitosis.

2.11. Orthotopic TNBC model

The orthotopic TNBC model was generated by injection of $1*10^6$ MDA-MB-231 cells in 50 μl Matrigel into the mammary fat pad of female BALB/c nude mice (5–7 weeks old; Charles River Laboratories, Frederick, MD). Mice were randomized into 4 groups of 8 mice prior to treatment start. Treatment was initiated when tumours reached approximately 70 mm³. Treatment groups were 1) vehicles for Vinblastine (saline) and Ispinesib (DMSO), 2) Vinblastine (1 mg/kg, in saline) plus DMSO, 3) Ispinesib (5 mg/kg, in DMSO) plus saline, and 4) Vinblastine (1 mg/kg, in saline) plus Ispinesib (5 mg/kg, in DMSO). Treatment was administered i.p. once a week for 3 weeks. Animal weights and tumour size were measured twice a week. Tumour volumes were calculated according to the formula $1/2*l*w^2$. Mice were sacrificed 8 weeks after treatment start. All experimental procedures involving mice were conducted in accordance with the guidelines of IACUC and the regulations of the Animal Research and Comparative Medicine Committee of Houston Methodist Research Institute.

2.12. Statistical analysis

Computational assignments were done using the student version of the computing environment Matlab (Version 7.8.0.347 (R2009a)). Statistical analysis of the CI was performed on results from growth inhibition assays using the software CalcuSyn version 2.1 (Biosoft, Cambridge, UK) (Chou and Hayball, 1996). Results from cell cycle and apoptosis assays were analysed by multiple comparisons between different treatment groups using one-way ANOVA (GraphPad Prism 5, GraphPad Software Inc., La Jolla, CA). Multiple comparisons between different treatment groups from the in vivo study were conducted using the Student's t-test (GraphPad Prism 5, GraphPad Software Inc., La Jolla, CA).

3. Results

3.1. Acquisition and multivariate analysis of compound-induced phenotypes in triple-negative breast cancer cells

A workflow was designed to identify synergistic drug combinations in TNBC cells (Figure 1). Thereby, HCS was used to simultaneously monitor cellular markers (i.e. DNA, F-actin, and microtubules) in MDA-MB-231-luc cells exposed to 55 FDA-approved drugs and biologically active compounds of 3 concentrations each (0.1, 1 and 10 μM) (Supplementary Table 1). Altogether, 3150 fluorescent images were captured, 1050 for each channel of the DNA-microtubule-actin marker set. Figure 2A shows MDA-MB-231-luc cells treated with doxorubicin and vinblastine for 24 h in comparison to control cells. The differentiation between drug-induced phenotypes was based on cellular features. The treatment shown here altered features describing cell shape and region properties compared to control. To allow for the extraction of feature values from images automatic image processing was conducted using a seeded watershed algorithm after conversion of RGB images into gray-scale images (Li et al., 2007). An example for segmentation of cells is shown in Figure 2B. On average, image segmentation resulted in 117 ± 32 and 114 ± 46 delineated cells for untreated control and compound treatment per view field, respectively, and a total of 120,361 segmented cells. Extracted features described region properties, intensity, shape, and texture characteristics of stained DNA and non-DNA regions for each cell (Supplementary Table 2) (Wang et al., 2009). Cellular image-based drug profiling was performed using a support vector machine (SVM) (Loo et al., 2006, 2007). SVM yielded best prediction power using 2-fold compared to leave-one-out, 5- and 10-fold cross-validation (CV) (data not shown), with average classification accuracies of over 80% for all 3 compound concentrations (Supplementary Figure 1).

To verify the model's accuracy, profile dissimilarities of compounds with the same molecular target were assessed. For example the majority of dissimilarities between the profiles of vinblastine and other compounds targeting the cytoskeleton were smaller than the average dissimilarity to all 152 compound profiles (Supplementary Figure 2A). The same applied to dissimilarities between compounds interacting with protein synthesis or degradation such as cycloheximide and emetine (Supplementary Figure 2B). This showed that profiles were associated with compound targets. Therefore, dissimilarities reflected the difference between compound-induced phenotypes and were used to predict potential synergistic combinations. Experimental evaluation of all pairwise combinations resulting from 55 compounds would require 1485 combination experiments, testing only one concentration per compound. To reduce this search space we selected compound pairs based on the hypothesis that combination of compounds with either very similar or dissimilar phenotypes would induce synergistic growth inhibition in TNBC cells. We used the SVM-derived profiles to select compound pairs with this characteristic.

Profile dissimilarities smaller or larger than the average dissimilarity to all 152 compound profiles were considered similar or dissimilar, respectively. The dot plot in Figure 2C
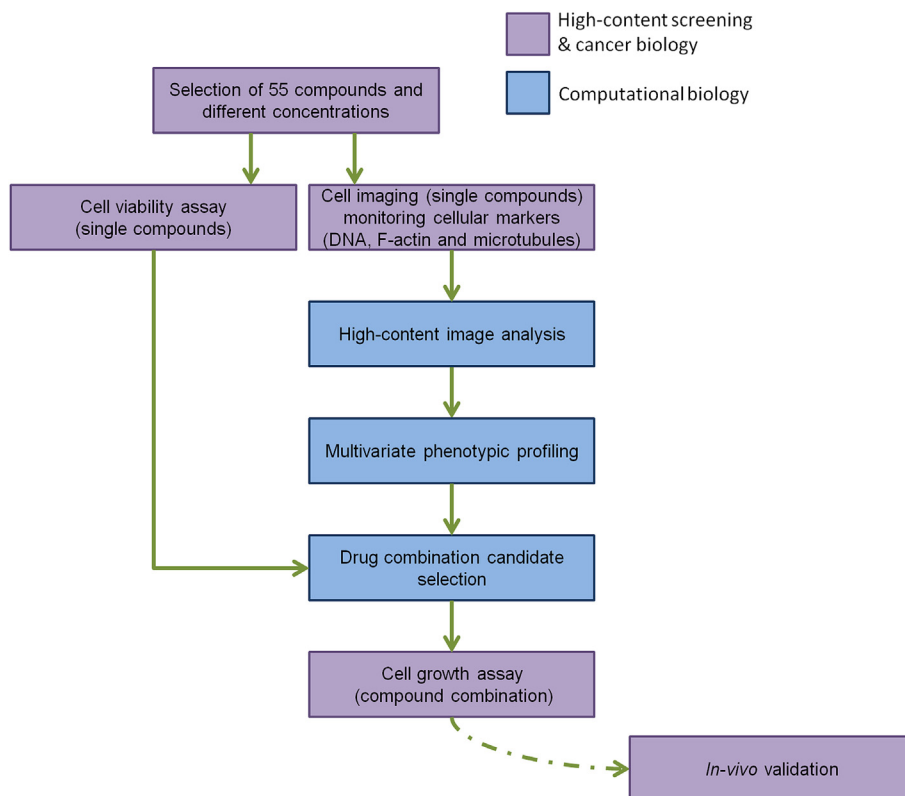
Figure 1 — Workflow for the image—based discovery of potential synergistic drug combination. High-content image analysis and compound profiling using a vector machine formed the basis for comparison of phenotypic outcome due to compound treatment. Combination pairs were selected for validation if compound profiles proved to be consistently similar or dissimilar. Subsequently, the effect of identified combination pairs on cell growth inhibition was measured. The assessment of the most promising synergistic combination pair was extended to an *in vivo* model of TNBC.

shows the profile dissimilarities of compound pairs after normalization to the average dissimilarity of all 152 profiles. Three of the compound pairs displaying similar profiles for the majority of dose pairs were cytochalasin D/vinblastine, SB203580/SC560, and cytochalasin D/cycloheximide. For example, for the compounds cytochalasin D/vinblastine, 8 out of 12 profile pairs had dissimilarities below the average dissimilarity to all compound profiles, indicating similar compound-induced phenotypes. Likewise, 7 out of 12 and 12 out of 16 profile pairs had dissimilarities smaller than the average dissimilarity for SB203580/SC560 and cytochalasin D/cycloheximide. In sharp contrast, large profile dissimilarities were found for compound pairs vinblastine/doxorubicin and vinblastine/monastrol. Dissimilarities between vinblastine and doxorubicin profiles all exceeded the average dissimilarities to their profiles, while 8 out of 12 profile pairs exceeded the average dissimilarities to monastrol and vinblastine profiles.

3.2. Profile dissimilarities identify compounds that inhibit TNBC cell growth synergistically

After selection of combination pairs with either very similar or dissimilar profiles, we assessed their effects on growth of TNBC cells. Surface plots illustrating MDA-MB-231-luc cell growth indicated that the 5 identified pairwise combinations vinblastine/cytochalasin D, SB203580/SC560, cycloheximide/

cytochalasin D, vinblastine/doxorubicin, and vinblastine/monastrol inhibited cell growth more potently than single compounds (Supplementary Figure 3A). Determining the Excess Over Highest Single Agent (EOHSA) allowed for the identification of potential synergistic interaction between compounds and was visualized in surface plots (Supplementary Figure 3B). Combination effects of selected compound pairs exceeded the effects of single compounds for the majority of tested concentrations. Combination effects were further evaluated using the combination index (CI) theorem (Chou and Talalay, 1984). This analysis confirmed our hypothesis that compound pairs with either very similar or dissimilar profiles have the potential to synergistically inhibit TNBC cell growth (Figure 2D). Furthermore, among the five selected combination pairs, vinblastine/monastrol showed synergism for more than 80% of dose pairs and displayed the strongest synergistic interactions.

3.3. Vinblastine and KSP/Eg5 inhibitors interact synergistically in TNBC cells, but not in normal fibroblasts

Since the synergism between vinblastine and monastrol was the most potent, the validation of combination effects of vinblastine with KSP/Eg5 inhibitors was further pursued. Due to moderate inhibitor activity and poor solubility of monastrol, the development of more specific KSP/Eg5 inhibitors was expedited (Gartner et al., 2005; Sarli et al., 2005). Therefore we used
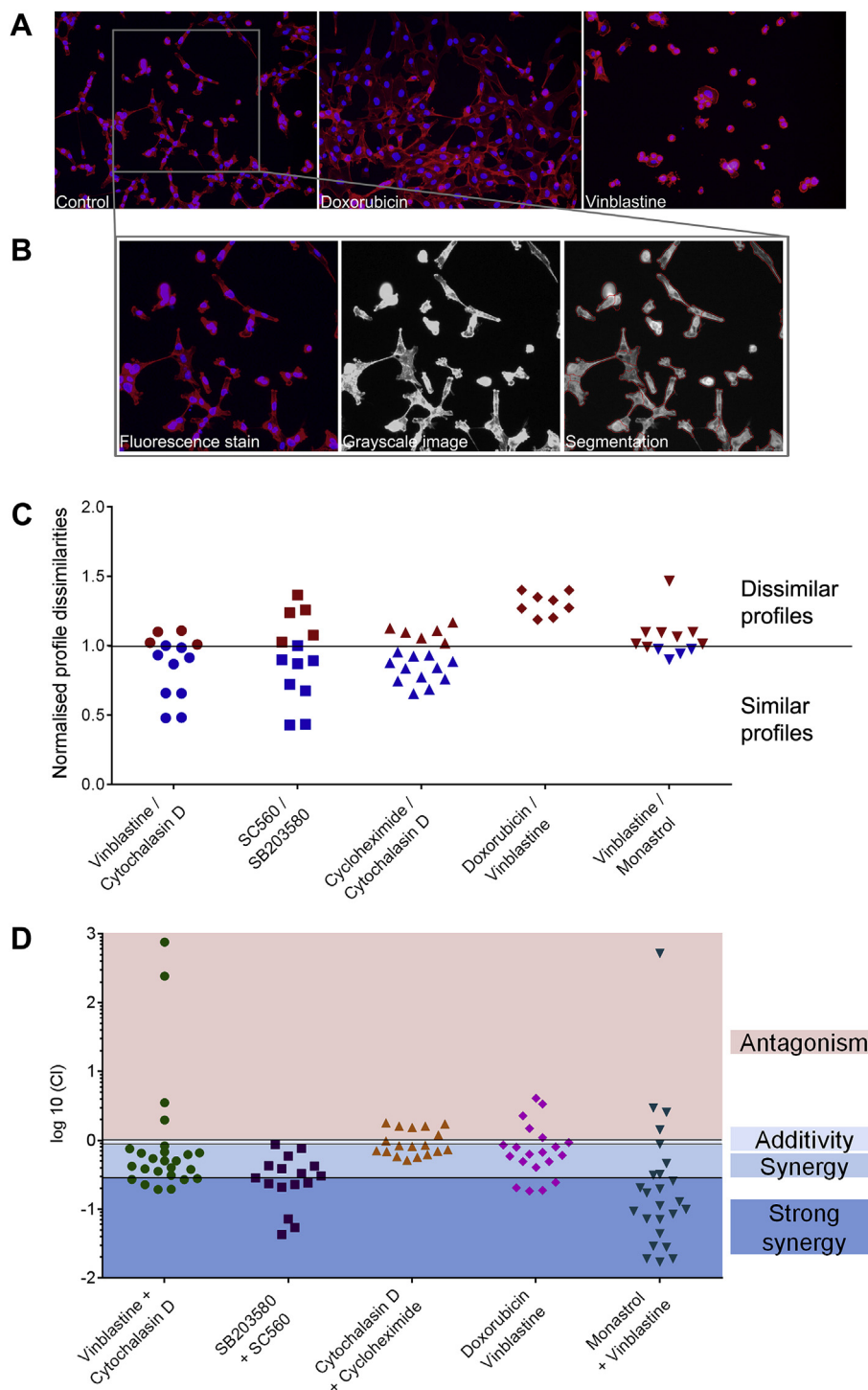
Figure 2 − Treatment−induced alterations of cellular phenotypes, image segmentation, and dissimilarities of compound profiles. A) Fluorescence staining of microtubule and DNA (channels overlaid), revealing some phenotypic alterations between untreated, 0.1 μM doxorubicin or 0.1 μM vinblastine treated MDA-MB-231-luc cells after 24 h. B) Delineation of single cells was conducted after conversion of RGB to grayscale images followed by image-segmentation using a seeded watershed algorithm. C) Dot plot representation of relative profile dissimilarity for compound pairs. Compound profiles were derived using an SVM. Profile dissimilarities were computed for each concentration pair using a distance measure and then normalized to the average dissimilarity of all compound profiles. D) Dot plot representation of the combination index (CI) for each compound pair. CI values were calculated for each concentration pairs following the Chou and Talalay method.

one of these compounds named ispinesib for combination experiments with vinblastine. Combination effects of monastrol/vinblastine and ispinesib/vinblastine were assessed in 3 independent TNBC cell lines using a 6 × 6 dose matrix including 5

individual concentrations of the single compounds and all their 25 dose pairs. Cell growth inhibition in MDA-MB-231, MDA-MB-468, and BT-549 cells was illustrated in surface plots and pointed towards an increased effect of the combination
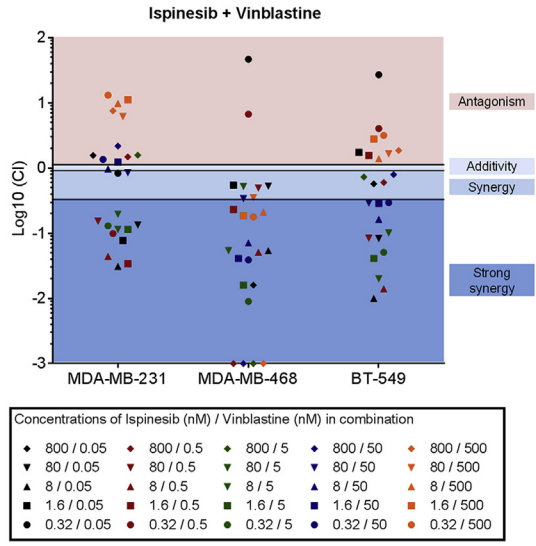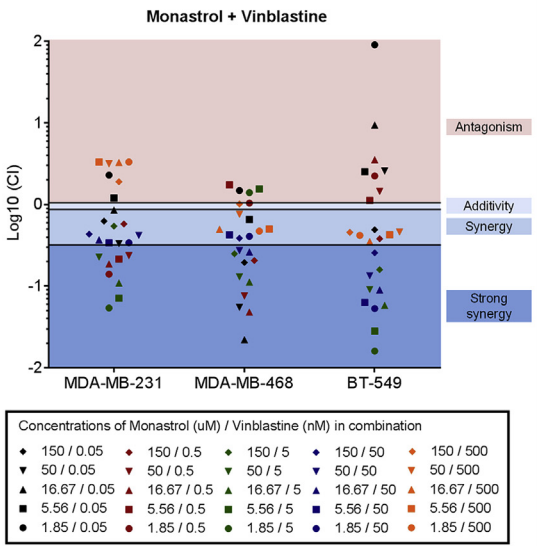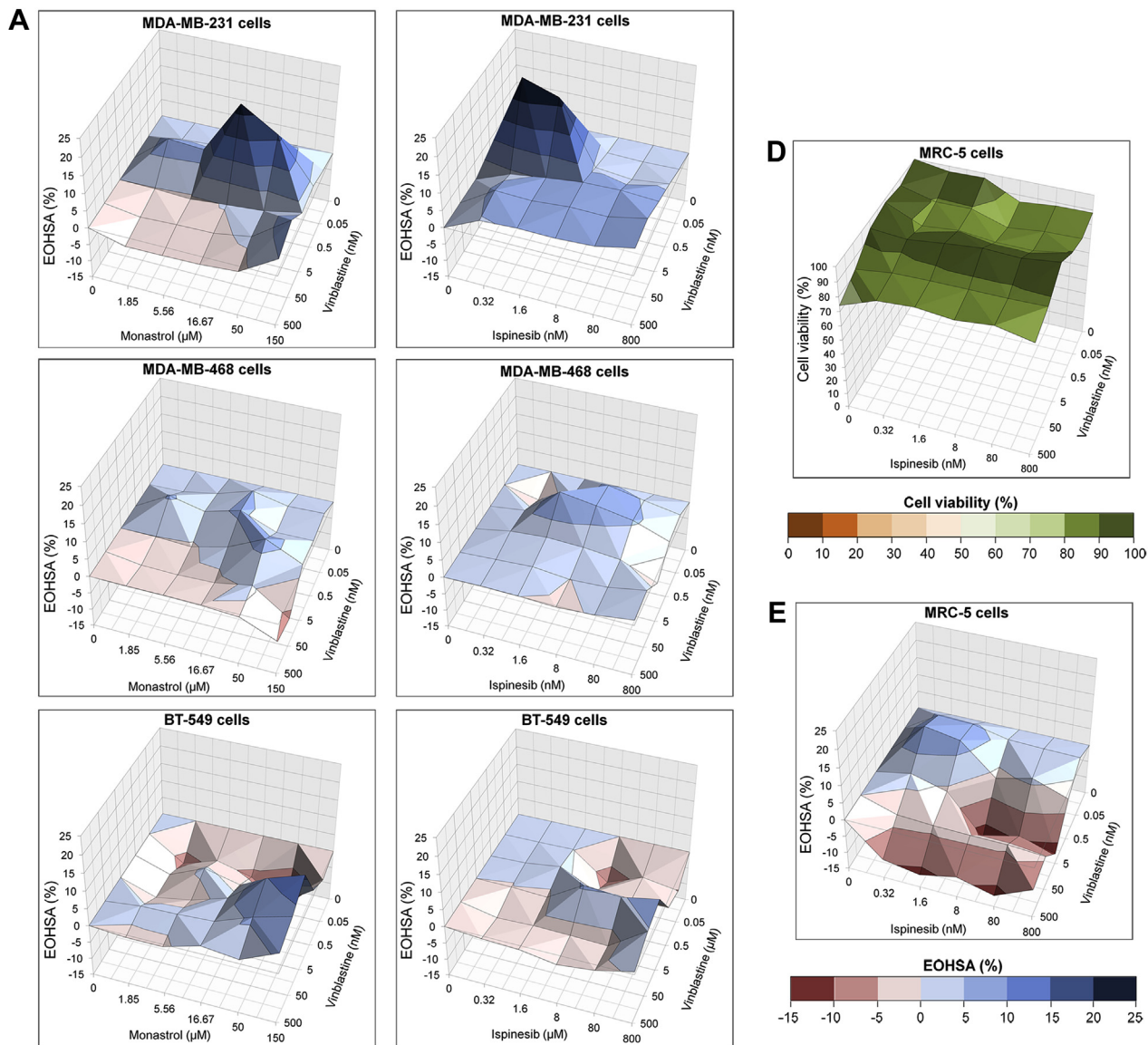
compared to single treatments after 72 h incubation (Supplementary Figure 4). Determining the EOHSA allowed for identification of combination effects exceeding the most effective single agent (Figure 3A). In MDA-MB-231 cells for example, combination treatment with monastrol and vinblastine exceeded cell growth inhibition compared to individual compounds for all but the combinations including high concentrations of vinblastine. The combination ispinesib/vinblastine was even more effective in this cell line and all 25 dose pairs exceeded cell growth inhibition compared to individual compounds. Quantitative assessment of combination effects using the CI theorem confirmed synergistic interactions for both combinations. On average more than 70% of the monastrol/vinblastine dose pairs synergistically inhibited TNBC cell growth (CI < 0.9), of which more than 50% induced strong synergism (CI ≤ 0.3) (Figure 3 B). Antagonistic interactions were mostly limited to either very high (MDA-MB-231 cells) or low (MDA-MB-468 and BT-549 cells) compound concentrations. Similar results were found for the combination ispinesib/vinblastine, for which on average more than 65% of dose pairs synergistically inhibited cell growth and more than 50% thereof inducing strong synergism (Figure 3C). Here, synergistic interactions were more prevalent in MDA-MB-231 and MDA-MB-468 cells compared to BT-549 cells. Antagonistic effects were mainly observed for combinations with either very low or high compound concentrations.

In sharp contrast with the effects observed in TNBC cells, ispinesib and vinblastine alone or in combination only induced a modest reduction in normal cell viability with a maximum of 20% inhibition (Figure 3D). The surface plot of the EOHSA indicated that dose pairs were predominantly antagonistic in normal fibroblasts, especially for higher compound concentrations, which were synergistic in TNBC cells (Figure 3E).

3.4. Synergism of vinblastine and KSP/Eg5 inhibitors is associated with increased mitotic arrest and apoptosis induction

Both vinblastine and KSP/Eg5 inhibitors were reported to induce mitotic arrest (Mayer et al., 1999; Pasquier and Kavallaris, 2008). We therefore investigated the impact of these compounds used alone and in combination on the cell cycle distribution of MDA-MB-231 cells. Cell cycle profiles indicated an increase in the percentage of cells in G2/M phase after 24 h of treatment with the combination in comparison to control cells, and cells treated with single vinblastine or ispinesib (Figure 4A). Precisely, treatment with 0.32 nM ispinesib

combined with 0.5 nM vinblastine significantly enhanced the G2/M arrest (46.0 ± 12.8%) compared to no treatment (17.3 ± 2.2%, $p < 0.0001$), ispinesib (18.4 ± 2.2%, $p < 0.0001$) or vinblastine (29.7 ± 6.3%, $p < 0.01$) only treatment (Figure 4B). Similar results were obtained with the combination of monastrol and vinblastine (Supplementary Figure 5).

The mechanism leading to a G2/M arrest differs between the compounds, with KSP/Eg5 inhibitors inducing the formation of monopolar mitotic spindles (Mayer et al., 1999), while vinblastine blocks cells at the metaphase to anaphase transition with either monopolar, bipolar or multipolar mitotic spindles (Ngan et al., 2001). To further decipher the combination mechanism, we assessed the induction of mitotic arrest and formation of mitotic spindles following single or combination treatment using immunofluorescence staining of microtubules. Figure 4C shows representative fluorescent images of MDA-MB-231 cell microtubules and DNA 24 h posttreatment. Exposure to 4 nM vinblastine induced mitotic arrest at the metaphase to anaphase transition with either monopolar or bipolar spindles. In comparison, mitotic arrest induced by ispinesib (4 nM) and the combination was characterised exclusively by the formation of monopolar mitotic spindles. Quantification of fluorescent images confirmed that the mitotic arrest induced by the combination was driven by the formation of monopolar spindles rather than an increase in bipolar spindles (Figure 4D), thus suggesting that vinblastine enhanced the ispinesib-induced phenotype.

The mitotic arrest of malignant cells is frequently associated with apoptotic cell death. Here, treatment of MDA-MB-231 cells with ispinesib (0.32 nM) and vinblastine (0.5 nM) in combination induced a 2.1−3.1-fold increase in apoptosis induction (27.2 ± 1.8%, $p < 0.0001$) as compared to untreated control (8.9 ± 1.0%, $p > 0.05$), vinblastine (13.1 ± 1.3%) or 0.32 nM ispinesib (12.2 ± 2.9%) alone (Figure 4E and F). Altogether, these findings proved that the combination treatment substantially enhanced apoptotic cell death in TNBC cells, as a result of a mitotic arrest.

3.5. Vinblastine synergizes with KSP/Eg5 inhibitors in an orthotopic model of TNBC

To investigate the *in vivo* antitumour activity in an orthotopic xenograft model of TNBC, tumor-bearing nude mice were treated with vehicle control, vinblastine alone (1 mg/kg), ispinesib alone (5 mg/kg), or their combination once a week for 3 weeks. Over the 8 week study period, no significant weight loss (>20% of the body weight) was observed in any of the groups and mice constantly gained weight (Figure 5A). Administration

---

Figure 3 − **Combination effects of KSP/Eg5 inhibitors and vinblastine on the growth of TNBC cells and normal fibroblasts. Effects of combination treatments were tested for 25 concentration pairs 72 h post-treatment. (A, B) Surface plots of the Excess Over Highest Single Agent (EOHSA) show the difference in cell growth inhibition between KSP/EG5 inhibitors/vinblastine in combination and the most potent single treatment at the corresponding concentration in three independent TNBC cell lines. Shades of blue depict positive values and thus stand for a greater effect of the combination compared to single agents. (B, C) Dot plot representations of the combination index (CI) for the combinations monastrol/vinblastine and ispinesib/vinblastine for all 25 concentration pairs each. CI values were calculated following the Chou and Talalay method. (D) Surface plots showing the cell viability of MRC-5 fibroblasts after treatment with ispinesib/vinblastine alone or in combination. Single compound concentrations are denoted on the x- and y-axis, and cell viability is plotted on the z-axis relative to control. (E) Surface plot of the Excess Over Highest Single Agent (EOHSA) shows the difference in cell viability between ispinesib/vinblastine in combination and the most potent single treatment at the corresponding concentration in MRC-5 cells.**
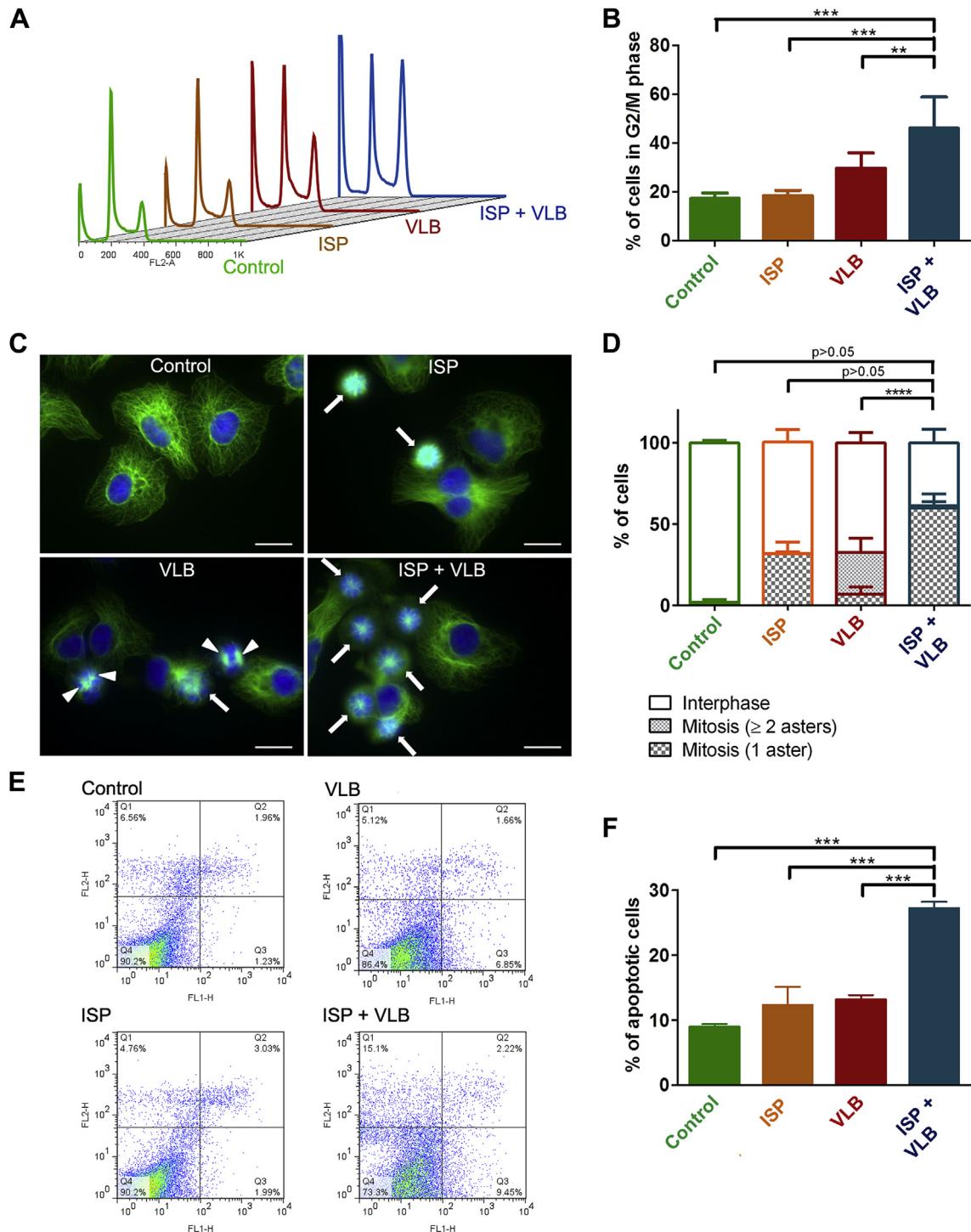
Figure 4 – Combination effects of ispinesib and vinblastine on cell cycle, mitotic spindle and apoptosis induction. (A) Representative cell cycle profiles of MDA-MB-231 cells incubated for 24 h with 0.5 nM vinblastine (red), 0.32 nM ispinesib (orange), or the combination (blue) measured using PI staining, and (B) quantification of the fraction of cells arrested in G2/M phase. *Columns*, means of at least 3 individual experiments; *Bars*, SD. Statistical analysis was performed using one-way ANOVA (**$p < 0.01$, ***$p < 0.001$). (C) Representative photographs of fluorescent staining of microtubules and nuclei in MDA-MB-231 cells 24 h post-treatment with 4 nM of ispinesib or vinblastine or their combination. Arrows and arrowheads denote mitotic cells with monoploar and bipolar spindles, respectively. *Scale bars*, 20 μm. (D) Quantification of mitotic cells with monopolar or bipolar mitotic spindles. *Columns*, average of at least 350 cells; *Bars*, SD. Statistical analysis was performed by comparing the number of mitotic cells with bipolar spindles using one-way ANOVA (****$p < 0.0001$). (E) Representative flow cytometry profiles of MDA-MB-231 cells and (F) quantification of apoptotic cells after 48 h treatment with 0.32 nM ispinesib and 0.5 nM vinblastine alone or in combination measured using Annexin V-FITC and PI staining. *Columns*, means of at least 3 individual experiments; *Bars*, SD. Statistical analysis was performed using one-way ANOVA (***$p < 0.001$).
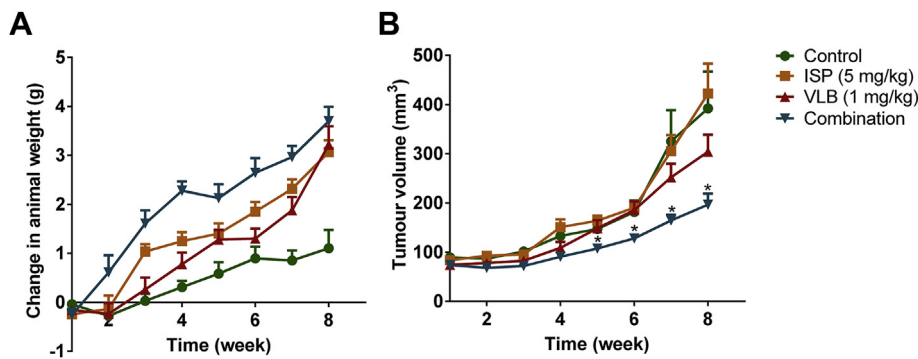
Figure 5 − **Change in animal weight and antitumour effect *in vivo*. Nude mice (BALB/c) were injected with 1*10⁶ MDA-MB-231 cells to establish an orthotopic TNBC model. Treatment with ispinesib (5 mg/kg) and Vinblastine (1 mg/kg) alone or in combination was initiated when the mean tumour volume reached about 70 mm³ and was administered i.p. weekly for three weeks. Mice were monitored for a period of 8 weeks. (A) Change in animal weights for the untreated control and treatment groups. (B) Antitumour effect of combination treatment and single treatments. Statistical analysis of the tumor volume between vinblastine only and the combination treatment was performed using the Student's *t*-test (****p* < 0.05). *Points*, mean values for 8 mice per group; *Bars*, SE.**

of ispinesib and/or vinblastine did not induce any noticeable side effects and was therefore well tolerated. Importantly, the synergism between vinblastine and ispinesib observed *in vitro* was reflected *in vivo* by an increased antitumour activity of the combination compared to single treatments (Figure 5B). From week 5 onwards, combination treatment significantly reduced tumour growth in mice, compared to control and single treatments (Supplementary Figure 6). At study completion, the tumour volume of the control group was on average 392 ± 299 mm³, those in the ispinesib and vinblastine only treated groups were 422 ± 244 mm³ and 304 ± 138 mm³, respectively, while that of the combination treated group was reduced to 197 ± 90 mm³. In summary, combination treatment significant delayed tumor growth by 49.8% ($p < 0.05$), 53.4% ($p < 0.01$), and 35.3% ($p < 0.05$) compared to vehicle control, ispinesib and vinblastine alone, respectively, confirming the enhanced antitumour activity against TNBC *in vivo*.

4. Discussion

Chemotherapeutic regimens consisting of multiple drugs improve therapeutic outcome and can overcome drug resistance (Dancey and Chen, 2006; Ramaswamy, 2007). However, most combinations currently used in the clinic have been developed through trial and error and this approach is expensive and is often met with limited success. To facilitate the rational design of combination chemotherapy regimens effective against drug-refractory tumours such as TNBC, we developed methodology based on high-content imaging and multivariate drug profiling. Our workflow integrated fluorescence microscopy, automatic image segmentation, and multivariate compound profiling, followed by evaluation of combination effects, and led to the identification of synergistic interactions that were validated in a preclinical model of TNBC.

Biological systems acquire robustness to external perturbations through several principles including systems control, redundancy and 'fail-safe-mechanism' (Kitano, 2004, 2007). In cancer cells this robustness is facilitated by genetic and epigenetic modifications. The resulting compensation mechanisms

often bypass the effect of single drugs and are the reasons for the failure of these single-drug treatments in complex disease such as cancer (Hartman et al., 2001; Jia et al., 2009; Kitano, 2007). Optimized multi-component therapies can surmount these defence mechanisms and are often used in clinic (Baguley and Kerr, 2002; Jia et al., 2009; Ramaswamy, 2007). Three mechanisms involved in triggering synergistic drug interactions were proposed. The first assumption is that components of drug cocktails act on the same pathway and therefore amplify the effect observed for single drug treatment. Secondly, compensatory mechanisms, which neutralise the effect of a single drug, are disabled by the diversity of the drug combinations. And the third possibility is that drugs of a combination act on different molecules or mutation sites to avoid cross-resistance (Kitano, 2007). Systems-oriented approaches are promising tools to develop such drug combinations. We explored the approach of combining compounds depending on the dissimilarities between the induced phenotypes. Phenotypic alterations are caused by the interruption of signalling pathways, which translates into changes in cell proliferation, morphology, and survival (Megason and Fraser, 2007). Here, we hypothesised that compounds inducing either very similar or dissimilar profiles have the potential to interact synergistically. Combinations of compounds with similar phenotypic effect can either amplify the inhibition of a single target or overcome compensatory mechanisms. Such compounds potentially act in the same or inter-connected pathways, or else interfere at different nodes in a pathway with a common downstream target. We found that compound pairs vinblastine/cytochalasin D, SB203580/SC560, and cycloheximide/cytochalasin D induced similar phenotypes and synergistically inhibited TNBC cell growth. As an example, vinblastine/cytochalasin D in combination might counteract compensatory mechanisms, such as accumulation of actin stress fibres induced by microtubule depolymerization (Enomoto, 1996; Pasquier et al., 2010) and reciprocally microtubule polymerization following disruption of actin filaments (Uematsu et al., 2007). In contrast, compounds that act on independent targets and thus entail the simultaneous disruption of diverse pathways are likely to induce different phenotypes. The disruption of several cellular pathways

affects the cellular robustness and explains the synergistic interaction of the combination. An example is the compound pair of FDA-approved chemotherapeutics doxorubicin and vinblastine, which are part of the standard of care for Hodgkin's lymphoma (Bonadonna et al., 1975) and were here found to induced synergistic TNBC cell growth inhibition. Although not all possible pair-wise combinations were examined in the present study, our results showed that compound pairs with either very similar or dissimilar profiles synergistically inhibited TNBC cell growth.

Despite being likely to have major clinical implications, many anti-cancer drug combinations have not been pre-clinically studied for the nature of their interaction or the dependencies of synergistic interactions (Chabner and Longo, 2006; Dancey and Chen, 2006), even though this type of interaction is known to be limited (Mayer and Janoff, 2007). In this study, the combination of Eg5/KSP inhibitors with vinblastine was selected for thorough analysis in TNBC models, as its synergistic interaction was the most potent compared to that of other tested compound pairs. Vinblastine is a microtubule-targeting anticancer agent, which interferes with microtubule dynamics, causing mitotic arrest and subsequent apoptotic cell death (Jordan and Wilson, 2004). It is used for the treatment of a broad range of cancers (Jackson et al., 2007; Jordan and Wilson, 2004), and was reported to have anticancer activity in pretreated patients with locally advanced and metastatic breast cancer (Ospovat et al., 2009). KSP/Eg5 inhibitors also cause mitotic arrest, which is, however, elicited by failure of bipolar microtubule spindle formation (Leizerman et al., 2004). The potential of KSP/Eg5 as an anticancer target was identified following the discovery of monastrol (Mayer et al., 1999), which prompted further development of this class of inhibitors (Rath and Kozielski, 2012). In the clinic, patients suffering from locally advanced or metastatic breast cancer showed promising response following the administration of ispinesib alone (Miller et al., 2005), or in combination with chemotherapeutic agents (Rodon et al., 2006). We found that synergistic interactions of KSP/Eg5 inhibitors and vinblastine were sustained for different doses and independent of the different sensitivities of TNBC cell lines to the single compounds. BT-549 cells were previously reported to be less sensitive to KSP/Eg5 inhibitors as compared to MDA-MB-231 and MDA-MB-468 cells (Purcell et al., 2010). This is important considering the cellular heterogeneity of tumours (Ramaswamy, 2007).

The synergism likely originates from the simultaneously induced, yet distinct mechanisms responsible for mitotic arrest and subsequently apoptotic cell death. Pritchard et al. explored different types of mechanisms involved in drug interactions and proposed that synergism was associated with the enhancement of a single-compound drug mechanism of action (Pritchard et al., 2013). This is in agreement with our finding that the ispinesib-induced phenotype (i.e. formation of monopolar mitotic spindle) is enforced through the addition of vinblastine leading to a significantly increased mitotic arrest and apoptosis induction compared to single compound treatments.

Synergistic interactions of drug combinations are only of clinical importance if their antitumour effect exceeds general toxicity and adverse synergistic effects observed in normal tissue (Ocana et al., 2012). We found that the synergistic interaction between ispinesib and vinblastine in rapidly dividing malignant TNBC cells was not translated into increased cytotoxicity in a model of normal fibroblasts. This might be associated with the greater selectivity of combinations compared to individual drugs and the dependence of synergistic interactions on pathways and cellular processes facilitating profitable drug interactions (Lehar et al., 2009). In support of our *in vitro* findings, the combination of ispinesib and vinblastine was not only well tolerated *in vivo*, but also showed enhanced antitumour activity as compared to single treatments. Altogether, these results demonstrate that the combination of KSP/Eg5 inhibitors with microtubule targeting agents has strong therapeutic potential and may lead to clinical benefits in TNBC patients.

5.   Conclusion

In summary, integrating image-based drug profiling and analysis coupled with rigorous experimental *in vitro* and *in vivo* validation can be used to discover new drug combinations for TNBC and other drug-refractory cancers. Drug profiling therefore represents a valid tool for the rapid and cost effective identification of synergistic drug combinations, and has broad applicability in a range of cancers to prioritize drug combinations for clinical trials.

Acknowledgements

Appendix A.
Supplementary data

Supplementary data related to this article can be found at http://dx.doi.org/10.1016/j.molonc.2014.06.007.

Disclosure of potential conflicts of interest

Authors have no conflict of interested to declare.

R E F E R E N C E S

Baguley, B.C., Kerr, D.J., 2002. Anticancer Drug Development. Academic Press, San Diego.

Bonadonna, G., Zucali, R., Monfardini, S., De Lena, M., Uslenghi, C., 1975. Combination chemotherapy of Hodgkin's disease with adriamycin, bleomycin, vinblastine, and imidazole carboxamide versus MOPP. Cancer 36, 252–259.

Borisy, A.A., Elliott, P.J., Hurst, N.W., Lee, M.S., Lehar, J., Price, E.R., Serbedzija, G., Zimmermann, G.R., Foley, M.A., Stockwell, B.R., Keith, C.T., 2003. Systematic discovery of multicomponent therapeutics. Proc. Natl. Acad. Sci. U. S. A. 100, 7977–7982.

Calzolari, D., Bruschi, S., Coquin, L., Schofield, J., Feala, J.D., Reed, J.C., McCulloch, A.D., Paternostro, G., 2008. Search algorithms as a framework for the optimization of drug combinations. PLoS Comput. Biol. 4, e1000249.

Carey, L.A., Dees, E.C., Sawyer, L., Gatti, L., Moore, D.T., Collichio, F., Ollila, D.W., Sartor, C.I., Graham, M.L., Perou, C.M., 2007. The triple negative paradox: primary tumor chemosensitivity of breast cancer subtypes. Clin. Cancer Res. – Off. J. Am. Assoc. Cancer Res. 13, 2329–2334.

Chabner, B., Longo, D.L., 2006. Cancer chemotherapy and Biotherapy: Principles and Practice, fourth ed. Lippincott Williams & Wilkins, Philadelphia.

Chang, C.-C., Lin, C.-J., 2001. LIBSVM: a Library for Support Vector Machines.

Chou, T.C., Hayball, M.P., 1996. CalcuSyn Version 2.1: Windows Software for Dose Effect Analysis. Biosoft, Cambridge, UK.

Chou, T.C., Talalay, P., 1984. Quantitative analysis of dose-effect relationships: the combined effects of multiple drugs or enzyme inhibitors. Adv. Enzyme Regul. 22, 27–55.

Dancey, J.E., Chen, H.X., 2006. Strategies for optimizing combinations of molecularly targeted anticancer agents. Nat. Rev. Drug Discov. 5, 649–659.

Enomoto, T., 1996. Microtubule disruption induces the formation of actin stress fibers and focal adhesions in cultured cells: possible involvement of the rho signal cascade. Cell Struct. Func. 21, 317–326.

Gartner, M., Sunder-Plassmann, N., Seiler, J., Utz, M., Vernos, I., Surrey, T., Giannis, A., 2005. Development and biological evaluation of potent and specific inhibitors of mitotic Kinesin Eg5. Chembiochem 6, 1173–1177.

Haffty, B.G., Yang, Q., Reiss, M., Kearney, T., Higgins, S.A., Weidhaas, J., Harris, L., Hait, W., Toppmeyer, D., 2006. Locoregional relapse and distant metastasis in conservatively managed triple negative early-stage breast cancer. J. Clin. Oncol. – Off. J. Am. Soc. Clin. Oncol. 24, 5652–5657.

Hartman, J.L.t., Garvik, B., Hartwell, L., 2001. Principles for the buffering of genetic variation. Science 291, 1001–1004.

Jackson, J.R., Patrick, D.R., Dar, M.M., Huang, P.S., 2007. Targeted anti-mitotic therapies: can we improve on tubulin agents? Nat. Rev. Cancer 7, 107–117.

Jia, J., Zhu, F., Ma, X., Cao, Z., Li, Y., Chen, Y.Z., 2009. Mechanisms of drug combinations: interaction and network perspectives. Nat. Rev. Drug Discov. 8, 111–128.

Jordan, M.A., Wilson, L., 2004. Microtubules as a target for anticancer drugs. Nat. Rev. Cancer 4, 253–265.

Kitano, H., 2004. Biological robustness. Nat. Rev. Gen. 5, 826–837.

Kitano, H., 2007. A robustness-based approach to systems-oriented drug design. Nat. Rev. Drug Discov. 6, 202–210.

Lehar, J., Krueger, A.S., Avery, W., Heilbut, A.M., Johansen, L.M., Price, E.R., Rickles, R.J., Short 3rd, G.F., Staunton, J.E., Jin, X., Lee, M.S., Zimmermann, G.R., Borisy, A.A., 2009. Synergistic drug combinations tend to improve therapeutically relevant selectivity. Nat. Biotechnol. 27, 659–666.

Leizerman, I., Avunie-Masala, R., Elkabets, M., Fich, A., Gheber, L., 2004. Differential effects of monastrol in two human cell lines. Cell Mol. Life Sci. 61, 2060–2070.

Li, F., Zhou, X., Ma, J., Wong, S.T., 2007. An automated feedback system with the hybrid model of scoring and classification for solving over-segmentation problems in RNAi high content screening. J. Microsc. 226, 121–132.

Liedtke, C., Mazouni, C., Hess, K.R., Andre, F., Tordai, A., Mejia, J.A., Symmans, W.F., Gonzalez-Angulo, A.M., Hennessy, B., Green, M., Cristofanilli, M., Hortobagyi, G.N., Pusztai, L., 2008. Response to neoadjuvant therapy and long-term survival in patients with triple-negative breast cancer. J. Clin. Oncol. – Off. J. Am. Soc. Clin. Oncol. 26, 1275–1281.

Loo, L.-H., Wu, L.F., Altschuler, S.J., 2006. Automated multivariate profiling of drug effects from fluorescence microscopy images. In: 3rd IEEE International Symposium on Biomedical Imaging: Nano to Macro, 2006, pp. 251–254.

Loo, L.H., Wu, L.F., Altschuler, S.J., 2007. Image-based multivariate profiling of drug responses from single cells. Nat. Methods 4, 445–453.

Mayer, L.D., Janoff, A.S., 2007. Optimizing combination chemotherapy by controlling drug ratios. Mol. Interv. 7, 216–223.

Mayer, T.U., Kapoor, T.M., Haggarty, S.J., King, R.W., Schreiber, S.L., Mitchison, T.J., 1999. Small molecule inhibitor of mitotic spindle bipolarity identified in a phenotype-based screen. Science 286, 971–974.

Megason, S.G., Fraser, S.E., 2007. Imaging in systems biology. Cell 130, 784–795.

Miller, K., Ng, C., Ang, P., Brufsky, A.M., Lee, S.C., Dees, E.C., Piccart, M., Verrill, M., Wardley, A., Loftiss, J., Bal, J., Yeoh, S., Hodge, J., Williams, D., Dar, M., Kathman, S., Ho, P.T.C., 2005. Phase II, open label study of SB-715992 (ispinesib) in subjects with advanced or metastatic breast cancer. In: 28th Annual San Antonio Breast Cancer Symposium, San Antonio (TX).

Nelander, S., Wang, W., Nilsson, B., She, Q.B., Pratilas, C., Rosen, N., Gennemark, P., Sander, C., 2008. Models from experiments: combinatorial drug perturbations of cancer cells. Mol. Syst. Biol. 4, 216.

Ngan, V.K., Bellman, K., Hill, B.T., Wilson, L., Jordan, M.A., 2001. Mechanism of mitotic block and inhibition of cell proliferation by the semisynthetic Vinca alkaloids vinorelbine and its newer derivative vinflunine. Molecular Pharmacology 60, 225–232.

Ocana, A., Amir, E., Yeung, C., Seruga, B., Tannock, I.F., 2012. How valid are claims for synergy in published clinical studies? Ann. Oncol.: Off. J. Eur. Soc. Med. Oncol./ESMO 23, 2161–2166.

Ospovat, I., Siegelmann-Danieli, N., Grenader, T., Hubert, A., Hamburger, T., Peretz, T., 2009. Mitomycin C and vinblastine: an active regimen in previously treated breast cancer patients. Tumori 95, 683–686.

Pasquier, E., Kavallaris, M., 2008. Microtubules: a dynamic target in cancer therapy. IUBMB Life 60, 165–170.

Pasquier, E., Sinnappan, S., Munoz, M.A., Kavallaris, M., 2010. ENMD-1198, a new analogue of 2-methoxyestradiol, displays both antiangiogenic and vascular-disrupting properties. Mol. Cancer Ther. 9, 1408–1418.

Pritchard, J.R., Bruno, P.M., Gilbert, L.A., Capron, K.L., Lauffenburger, D.A., Hemann, M.T., 2013. Defining principles of combination drug mechanisms of action. Proc. Natl. Acad. Sci. U. S. A. 110, E170–E179.

Purcell, J.W., Davis, J., Reddy, M., Martin, S., Samayoa, K., Vo, H., Thomsen, K., Bean, P., Kuo, W.L., Ziyad, S., Billig, J., Feiler, H.S., Gray, J.W., Wood, K.W., Cases, S., 2010. Activity of the kinesin spindle protein inhibitor ispinesib (SB-715992) in models of breast cancer. Clin. Cancer Res. – Off. J. Am. Assoc. Cancer Res. 16, 566–576.

Ramaswamy, S., 2007. Rational design of cancer-drug combinations. N. Engl. J. Med. 357, 299–300.

Rath, O., Kozielski, F., 2012. Kinesins and cancer. Nat. Rev. Cancer 12, 527–539.

Reis-Filho, J.S., Tutt, A.N., 2008. Triple negative tumours: a critical review. Histopathology 52, 108–118.

Rodon, J., Till, E., Patnaik, A., Takimot, C., Kathmanz, S., Williams, D., Vasist, L., Bowen, C., Hodge, J., Dar, M., Tolcher, A., 2006. Phase I study of lspinesib in combination with capecitabine in patients with advanced solid tumors. In: 8th Annual EORTC-NCI-AACR Symposium on Molecular Targets and Cancer Therapeutics, Prague, Czech Republic.

Sarli, V., Huemmer, S., Sunder-Plassmann, N., Mayer, T.U., Giannis, A., 2005. Synthesis and biological evaluation of novel EG5 inhibitors. Chembiochem 6, 2005–2013.

Simmons, J.K., Patel, J., Michalowski, A., Zhang, S., Wei, B.-R., Sullivan, P., Gamache, B., Felsenstein, K., Kuehl, W.M., Simpson, R.M., Zingone, A., Landgren, O., Mock, B.A., 2014. TORC1 and class I HDAC inhibitors synergize to suppress mature B cell neoplasms. Mol. Oncol. 8, 261–272.

Uematsu, Y., Kogo, Y., Ohishi, I., 2007. Disassembly of actin filaments by botulinum C2 toxin and actin-filament-disrupting agents induces assembly of microtubules in human leukaemia cell lines. Biol. Cell 99, 141–150.

Wang, J., Zhou, X., Li, F., Bradley, P.L., Chang, S.F., Perrimon, N., Wong, S.T., 2009. An image score inference system for RNAi genome-wide screening based on fuzzy mixture regression modeling. J. Biomed. Inform. 42, 32–40.

Wong, P.K., Yu, F., Shahangian, A., Cheng, G., Sun, R., Ho, C.M., 2008. Closed-loop control of cellular functions using combinatory drugs guided by a stochastic search algorithm. Proc. Natl. Acad. Sci. U. S. A. 105, 5105–5110.

Zimmermann, G.R., Lehar, J., Keith, C.T., 2007. Multi-target therapeutics: when the whole is greater than the sum of the parts. Drug Discov. Today 12, 34–42.

Zinner, R.G., Barrett, B.L., Popova, E., Damien, P., Volgin, A.Y., Gelovani, J.G., Lotan, R., Tran, H.T., Pisano, C., Mills, G.B., Mao, L., Hong, W.K., Lippman, S.M., Miller, J.H., 2009. Algorithmic guided screening of drug combinations of arbitrary size for activity against cancer cells. Mol. Cancer Therap. 8, 521–532.